

## Electrical excitation of color centers in *n*-type diamond Schottky diodes

Florian Sledz<sup>1,\*</sup>, Igor A. Khramtsov<sup>2</sup>, Assegid M. Flatae<sup>1</sup>, Stefano Lagomarsino,<sup>3</sup>  
 Silvio Sciortino<sup>3,4,5</sup>, Shannon S. Nicley<sup>6,7</sup>, Rozita Rouzbahani<sup>6</sup>, Paulius Pobedinskas<sup>6</sup>,  
 Tianxiao Guo,<sup>8</sup> Xin Jiang,<sup>8</sup> Paul Kienitz<sup>9</sup>, Peter Haring Bolivar<sup>9</sup>, Ken Haenen<sup>10</sup>,  
 Dmitry Yu. Fedyanin,<sup>1,2</sup> and Mario Agio<sup>1,5</sup>

<sup>1</sup>*Laboratory of Nano-Optics, University of Siegen, Siegen, Germany*

<sup>2</sup>*Moscow Center for Advanced Studies, Moscow, Russia*

<sup>3</sup>*Sezione di Firenze, Istituto Nazionale di Fisica Nucleare, Sesto Fiorentino, Italy*

<sup>4</sup>*Department of Physics and Astronomy, University of Florence, Sesto Fiorentino, Italy*

<sup>5</sup>*National Institute of Optics (INO), National Research Council (CNR), Sesto Fiorentino, Italy*

<sup>6</sup>*Institute for Materials Research (IMO) & IMOMEC, Hasselt University & IMEC vzw, Diepenbeek, Belgium*

<sup>7</sup>*Department of Electrical and Computer Engineering, Michigan State University, East Lansing, USA*

<sup>8</sup>*Lehrstuhl für Oberflächen- und Werkstofftechnologien, University of Siegen, Siegen, Germany*

<sup>9</sup>*Group of Graphene-based Nanotechnology, University of Siegen, Siegen, Germany*

(Received 6 August 2024; revised 30 January 2025; accepted 16 April 2025; published 23 May 2025)

Color centers in diamond are promising systems for quantum technologies and nanophotonics as they are photostable emitters at room and elevated temperatures. The possibility of their electrical excitation has already been demonstrated within *p-i-n* diodes. However, this requires the growth of complex diamond structures. In contrast to these conventional approaches, we demonstrate the emission from color centers under electrical pumping in a Schottky diode configuration based on *n*-type diamond. Hydrogen passivation allows the modification of the Schottky barrier height and improves the injection of minority charge carriers needed for the electrical pumping, while electrons are provided by the *n*-type layer.

DOI: 10.1103/PhysRevApplied.23.054060

### I. INTRODUCTION

Among the fundamental building blocks of optical quantum technologies, quantum-light sources play a crucial role. So far, a wide range of light sources has been implemented, such as atoms, trapped ions, molecules, color centers in wide bandgap materials, and quantum dots [1–10]. Each source offers advantages and disadvantages. For instance, epitaxial quantum dots show atomlike emission characteristics. However, their stable operation requires cryogenic conditions and exhibits fluorescence fluctuations. In contrast to this possibility, color centers in diamond show stable emission properties at ambient and even high temperatures [11]. It has been demonstrated that color centers in diamond can produce photon emission rates that can reach more than  $10^6$  counts per second (cps) per color center under optical excitation [6].

However, from a practical point of view, it is highly desirable to control them under electrical excitation to develop a scalable quantum photonic architecture [12,13]. Electrical excitation not only avoids the use of bulky lasers but also provides the possibility to independently manipulate the emitters at the same time within large-scale integrated photonic circuits. However, the electrical excitation of color centers in diamond is very challenging. First, diamond is a unique material between semiconductors and insulators that features a bandgap energy ( $E_g$ ) of 5.47 eV. Therefore, it is extremely difficult to create a high density of free carriers, especially electrons, due to the high activation energy of dopants [14,15]. Second, the common approach for the electrical excitation of color centers in diamond is forward-biased *p-i-n* diodes that contain a color center in the *i*-type region [16–20]. Electrons injected from the *n*-type region and holes injected from the p-type region recombine at the color center, which results in photon emission [21,22]. However, the fabrication of diamond *p-i-n* diode is much more complicated than the fabrication of such a structure based on conventional semiconductors such as Si and GaAs. This is mainly due to the absence of an efficient technique for creating regions with high free carrier densities by ion implantation, which is used

\*Contact author: Florian.Sledz@uni-siegen.de

Published by the American Physical Society under the terms of the [Creative Commons Attribution 4.0 International license](#). Further distribution of this work must maintain attribution to the author(s) and the published article's title, journal citation, and DOI.

in microelectronics for low-cost production of integrated electronic circuits [23].

Here, we propose and experimentally demonstrate a fundamentally different approach for the electrical excitation of color centers in diamond, which provides the possibility to fabricate any number of independently operating devices on a single chip and, therefore, to develop scalable photonic circuits. In contrast to the common methods based on *p-n* and *p-i-n* structures, our approach is based on a Schottky barrier diode on *n*-type diamond (phosphorus-doped) [24]. The Schottky barrier height is modified by hydrogen passivation of the diamond surface to improve the injection of minority charge carriers (holes) needed for the electrical pumping, while electrons are directly provided by *n*-type diamond. This dramatically simplifies the fabrication and avoids complicated processes of structuring and regrowing of diamond. Diodes of any size can be created anywhere on a chip by performing appropriate metallization, which reduces the fabrication cost and leads to unprecedented scalability. Our findings are also relevant for obtaining an electrically pumped single-photon source.

## II. DEVICE CONCEPT AND NUMERICAL SIMULATIONS

Schottky diodes are known as majority carrier devices, i.e., the density of one type of free charge carriers (electrons and holes) is many orders of magnitude lower than the density of the other type at any point of the device at any bias voltage. Thus, the electron-hole recombination rate at the color center should be zero in Schottky diodes, which does not allow the efficient excitation of the color centers electrically. Although it is still possible to observe electroluminescence in such devices due to impact excitation, it is less efficient and usually requires large bias voltages of hundreds of volts [25,26]. Nevertheless, in the 1960s, it was theoretically shown that minority carriers can be injected directly from the metal to the semiconductor, if the Schottky barrier height (SBH) is comparable with or higher than the bandgap of the semiconductor [27]. The problem is that almost no material satisfies this requirement [28] due to the surface states at the metal-semiconductor interface, which pin the Fermi level [29] and have a large influence on the achievable barrier height.

Recently, it has been theoretically predicted that hydrogen termination of the diamond surface could dramatically reduce the density of surface states [30] and, therefore, their influence on the barrier height vanishes. Since the electron affinity of diamond is negative (down to  $\chi_e = -2.01$  eV) [31], the SBH can almost be equal to or higher than the bandgap energy of diamond, if the work function of the metal is sufficiently high. In this work, we use gold since it features one of the largest work functions (up to  $\Phi_M = 5.3$  eV) [32]. The theory predicts the SBH between gold and hydrogen-terminated *n*-type diamond,  $\Phi_{B,e}$ , to be

higher than 4.95 eV [30]. Accordingly, the SBH for holes  $\Phi_{B,h} = E_g - \Phi_{B,e}$  is less than 0.5 eV. Such a low potential barrier for holes gives the possibility to inject a significant density of holes, which are minority carriers in *n*-type diamond, directly from gold under high forward bias. Hence, high densities of both electrons and holes can be created near the Schottky contact, which can recombine at the color center at a high rate and efficiently excite it. A band structure of such a Schottky junction is shown in Fig. 1(a) in thermal equilibrium (top) and under forward bias (bottom). As electrons and holes are present in the vicinity of a color center, they can pump it into an excited state from which it can return to the ground state by the emission of a photon [21].

Self-consistent numerical simulations of the proposed structure have been performed using the software Silvaco TCAD. For the simulation, a free-standing *n*-type (phosphorus-doped) diamond film with a thickness ( $h$ ) of 2.2  $\mu\text{m}$ , a high donor concentration of  $10^{18} \text{ cm}^{-3}$ , a compensation ratio of 10%, and mobilities of  $\mu_n = \mu_p = 390 \text{ cm}^2 \text{ V}^{-1} \text{ s}^{-1}$  were used to consider the high doping level of the thin film [33]. On top of the diamond, an ohmic and a Schottky contact are placed with a spacing ( $d_n$ ) of 10  $\mu\text{m}$  in between, which are defined as boundary conditions at the edge of the simulation region. The simulations show an effective injection of holes by thermionic emission under large bias voltages. If the barrier height for holes is smaller than 0.4 eV, the hole current can even surpass the electron current. This can be seen as a second step in the *IV* curves in Fig. 1(b). At room temperature, the charge carrier capture is the limiting process of the luminescence dynamics, with capture rates of  $c_n n$  and  $c_p p$  less than  $10^6 \text{ s}^{-1}$ . Here  $c_n = 1.7 \times 10^{-8} \text{ cm}^3 \text{ s}^{-1}$  and  $c_p = 3.9 \times 10^{-7} \text{ cm}^3 \text{ s}^{-1}$  are the capture rate constants for the electrons and holes, respectively. According to references [21,22], the single-photon emission rates can then be calculated from the charge carrier densities  $n$  and  $p$  for electrons and holes, respectively, via

$$R = \eta \left( \frac{1}{c_n n} + \frac{1}{c_p p} \right)^{-1}. \quad (1)$$

Here,  $\eta$  is the quantum efficiency of the respective color center. Figures 1(c) and 1(d) show the single-photon emission rates of a single-color center with unity quantum efficiency ( $\eta = 1$ ) for Schottky barrier heights for holes of 0.1 and 1.0 eV at a forward bias voltage of 10 V, which leads to total current densities of  $j = 5.3$  and  $1.6 \times 10^{-2} \text{ A/cm}^2$ , respectively. Under these conditions, the maximal emission rates of 150 kcps and 60  $\mu\text{cps}$  are expected from a single emitter with  $\eta = 1$  located near the Schottky junction for the different configurations. While the maximal emission rate for a small barrier height for holes [Fig. 1(c)] is comparable with optical excitation rates [34], the maximum value for the large barrier

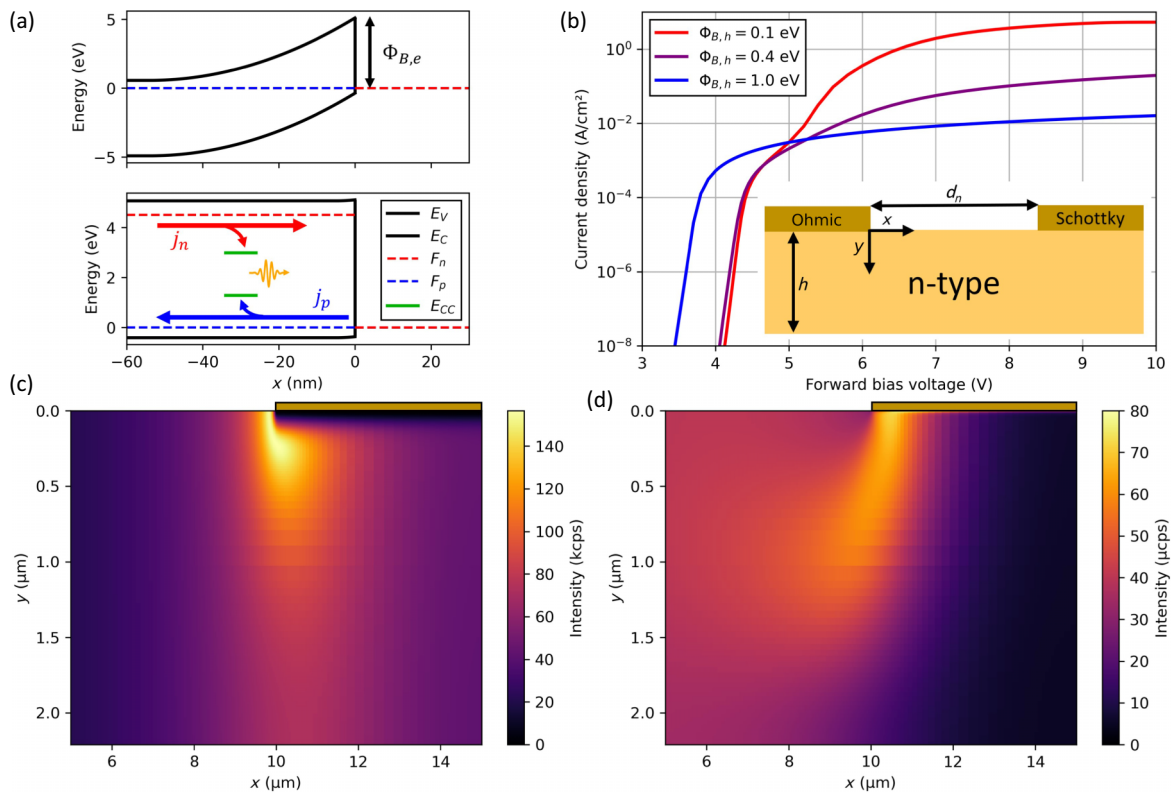


FIG. 1. (a) Schematic energy diagram of a Schottky junction with a barrier height of 5.1 eV in equilibrium (top) and a forward bias voltage of 4.5 V (bottom). The black lines show the valence ( $E_V$ ) and conduction bands ( $E_C$ ), while the red and blue dashed lines show the positions of the quasi-Fermi levels for electrons ( $F_n$ ) and holes ( $F_p$ ), respectively. The blue and red arrows (bottom) show the direction of the electron ( $j_n$ ) and hole current densities ( $j_p$ ). A small portion of the charge carriers are captured by color centers (energy levels  $E_{CC}$  shown in green), which leads to the emission of a photon (orange). (b) Simulated current-voltage characteristics for different Schottky barrier heights for holes,  $\Phi_{B,h}$ . For  $\Phi_{B,h}$  below 0.4 eV, an effective injection of holes can be seen as a step in the  $IV$  curve at  $\sim 5$  V. The inset shows the schematic of the simulated structure. The coordinate system is fixed to the edge of the ohmic contact. More details can be found in the text. Single-photon emission rates [based on Eq. (1)] of an ideal single-color center with 100% quantum efficiency placed at different depths ( $y$ ) and distances ( $x$ ) close to a Schottky contact with a bias voltage of 10 V and barrier heights for holes of (c) 0.1 and (d) 1.0 eV. The position of the Schottky contacts is marked with the boxes above the color maps.

height [Fig. 1(d)] is much lower than typical dark counts and noise levels, and it makes the observation of single-photon emission at such large barrier heights practically impossible. Additionally, one must consider the quantum efficiencies of the color centers and the collection and detection efficiencies of the experimental setup, such that less than 1% of the excitation results in a detected photon during the experiment.

### III. SAMPLE PREPARATION

#### A. Diamond growth

A phosphorus-doped homoepitaxial diamond film was grown on top of the surface of a (111)-oriented  $2.5 \text{ mm} \times 2.5 \text{ mm} \times 0.5 \text{ mm}$  type Ib high-pressure high-temperature (HPHT) diamond substrate (Sumitomo) by microwave plasma enhanced chemical vapor deposition (MW PE CVD) in a 2.45-GHz ASTeX PDS17 CVD reactor. The nitrogen content in the substrate is in the order

of  $10^{19} \text{ cm}^{-3}$ . During the growth, a total flow rate of 500 sccm and a pressure of 140 Torr were kept constant. The hydrogen ( $H_2$ ) rich plasma contained 0.15% of methane ( $CH_4$ ). For the incorporation of phosphorus, phosphine ( $PH_3$ ) was introduced into the plasma with a constant ratio of  $PH_3 : CH_4 = 5000$  ppm. The substrate temperature was maintained at  $1000^\circ\text{C}$  via a variation of the applied microwave power between 1.0 and 1.3 kW. The  $H_2$  and  $CH_4$  gasses are filtered to a purity of  $< 1$  ppb, while the  $PH_3$  is obtained from a source diluted to 200 ppm in  $H_2$ . After a growth time of eight hours, an  $n$ -type layer with a thickness of  $2.2 \pm 0.2 \mu\text{m}$  was obtained. The sample thickness was measured by a Mitutoyo Linear Gage (Model 542–158) [35].

#### B. Color center creation

Silicon ion implantation allowed us to create silicon-vacancy ( $SiV$ ) color centers and vacancies for nitrogen-vacancy ( $NV$ ) color centers. Thermal annealing enables

the activation of both centers. At first, the Si ions were implanted in the first 200 nm of the *n*-type layer by ion-beam implantation with different ion doses (i.e.,  $5 \times 10^7$ ,  $10^{12}$ ,  $10^{13}$ , and  $10^{14} \text{ cm}^{-2}$ ). The Si ion implantation is based on a 3 MV Tandetron accelerator equipped with an HVEE860 negative sputter ion source. Based on the charge state and terminal voltage, the Si ion species ( $\text{Si}^+$ ,  $\text{Si}^{2+}$ , and  $\text{Si}^{3+}$ ) can be accelerated to energies up to 10 MeV [36]. Two aluminum foils with a total thickness of 4.6  $\mu\text{m}$  have been used to reduce the ion energy to a few tens of kiloelectron volts to allow for the desired shallow implantation. Utilizing a home-built furnace, the sample was thermally annealed at a temperature of 1200 °C for  $\sim 1$  h under high-vacuum conditions ( $\sim 10^{-7}$  mbar) to enable the activation of the color centers. Besides the activation of the SiV color centers, the created vacancies also recombine with the incorporated N atoms during thermal annealing. This results in the formation of NV color centers within the *n*-type diamond layer. Based on an optical measurement using a known defect concentration of SiV color centers, the concentration of NV color centers in the *n*-type layer is assumed to be on the order of  $10^{16} \text{ cm}^{-3}$  (see Supplemental Material) [37]. Details on the optical studies of the color centers in the *n*-type sample can be found in a previous publication [34].

### C. Device fabrication

Before device fabrication, the sample was cleaned in acetone and isopropanol at  $\sim 50$  °C to remove organic contamination from its surface. In the first fabrication step, a lithographic mask was created on the cleaned diamond surface, followed by thermal evaporation of titanium (16 nm) and gold (150 nm). The contacts were structured by a lift-off process such that a single pad was formed in the different implanted regions. Within these contact pads, holes

TABLE I. Process parameters of the hydrogen plasma treatment.

Power	Temperature	Pressure	H <sub>2</sub> flow rate	Time
850 W	850 °C	20–26 torr	400 sccm	45 min

with a diameter of 100  $\mu\text{m}$  and pitch of 125  $\mu\text{m}$  were left blank for the formation of the Schottky contacts.

Next, the sample was transferred to another CVD reactor (ASTeX) for hydrogen plasma treatment of the diamond surface. The conditions of the plasma treatment are listed in Table I. The pressure was adjusted in the given bounds to stabilize the temperature to 850 °C during the treatment time.

After treatment, the sample was placed in the hydrogen atmosphere for  $\sim 2.5$  h to cool to room temperature. This plasma treatment has two effects: first, the ohmic contacts are thermally annealed by the formation of titanium-carbide at these high temperatures and, second, the diamond surface acquires a reduced electron affinity via the hydrogen passivation [38] and, thus, a lowering of the achievable barrier height for the holes. The recipe was tested by the formation of a surface conductive layer on an intrinsic diamond (see Supplemental Material) [37].

After cooling, the sample was removed from the CVD reactor and transferred to a thermal evaporation chamber for the deposition of the Schottky contact. For this, a 150-nm-thick gold layer was deposited over the whole sample without an additional adhesion layer, as the latter would affect the properties of the Schottky junction.

For the patterning of the final devices, a complementary positive lithographic mask was aligned relative to the ohmic contacts, which were visible beneath the gold layer. The gold in the undesired regions was wet etched using KI<sub>2</sub>/I<sub>2</sub> solution (Micro chemicals) for 2 min. This resulted

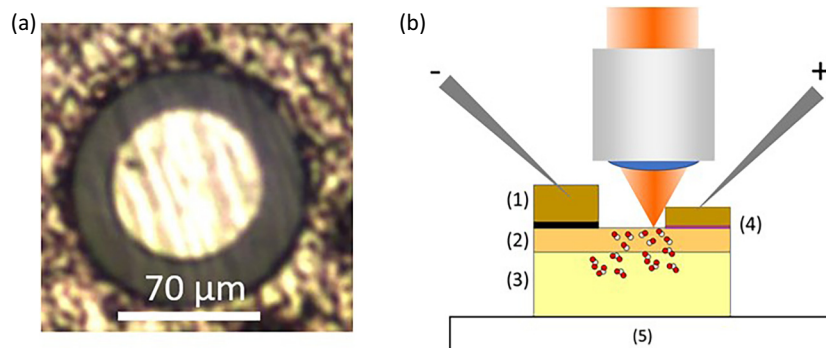


FIG. 2. (a) Microscope image of a single diamond Schottky light emitting diode. The inner disk is the Schottky contact with a diameter of 70  $\mu\text{m}$  and the surrounding (rough) contact is a joint ohmic contact. (b) Illustration of the fabricated and probed diamond Schottky light emitting diode and the measurement setup. The diode consists of (1) an ohmic contact (gold on titanium carbide), (2) the *n*-type diamond layer, (3) the HPHT substrate, and (4) the Schottky contact (gold on the hydrogen-passivated diamond). The red and white circles mark nitrogen atoms and vacancies in the different diamond layers, respectively. The sample is placed on (5) a Peltier element for heating of the sample.

in circular Schottky contacts with a diameter of 70  $\mu\text{m}$  surrounded by a common ohmic contact with circular holes with a diameter of 100  $\mu\text{m}$  [Fig. 2(a)].

#### IV. EXPERIMENTAL SETUP

The electroluminescence measurements were performed using a home-built  $\mu$ -photoluminescence optical setup. The setup consists of a 532 nm, 5 mW laser diode (Thorlabs) for optical excitation to localize the emitters for electrical excitation. The large working distance microscope objective (Zeiss LD C Epiplan-APOCHROMAT 50 $\times$ , 0.6 NA) collects the emitted signal. A compromise is made between a high numerical aperture for collection and a large working distance to avoid contact between the optics and the electrical probes. The collection optics, together with the spectroscopic approach, limit the emission optical plane to the  $n$ -type region, which has a depth of 2  $\mu\text{m}$  (see Supplemental Material [37]). The collected light is sent to a CMOS camera (Andor Zyla 4.2Plus) for wide-field imaging and, using a flip mirror, it is also coupled into a multimode fiber connected to a spectrometer (OceanOptics Flame 2000).

The diamond sample with fabricated devices on the surface was placed on top of a home-built sample holder with a Peltier heater, allowing for the thermal activation of free electrons in the  $n$ -type layer by heating the sample to 150 °C during the experiment. The Schottky and ohmic contacts were connected to a source measure unit (Keithley 2450) via two piezo micro probers (Imina Technologies miBots), which enabled the addressing of all the devices independently. Here, the cathode is placed on a joint ohmic contact pad for different devices in one implanted region, while the anode is positioned at the center of the Schottky contact. Figure 2(b) shows a sketch of this approach.

#### V. RESULTS AND DISCUSSION

##### A. IV characteristics

A set of  $IV$  curves is recorded in the region implanted with a Si dose of  $10^{12} \text{ cm}^{-2}$  at temperatures in the range of 25–150 °C. The measurements show a clear diode behavior with a highly temperature-dependent forward bias current and a reverse current, which is mainly given by the parallel currents through the measurement devices [Fig. 3(a)]. The shift of the zero crossing of the current at lower voltages is given by the discharge of an internal capacitor of the

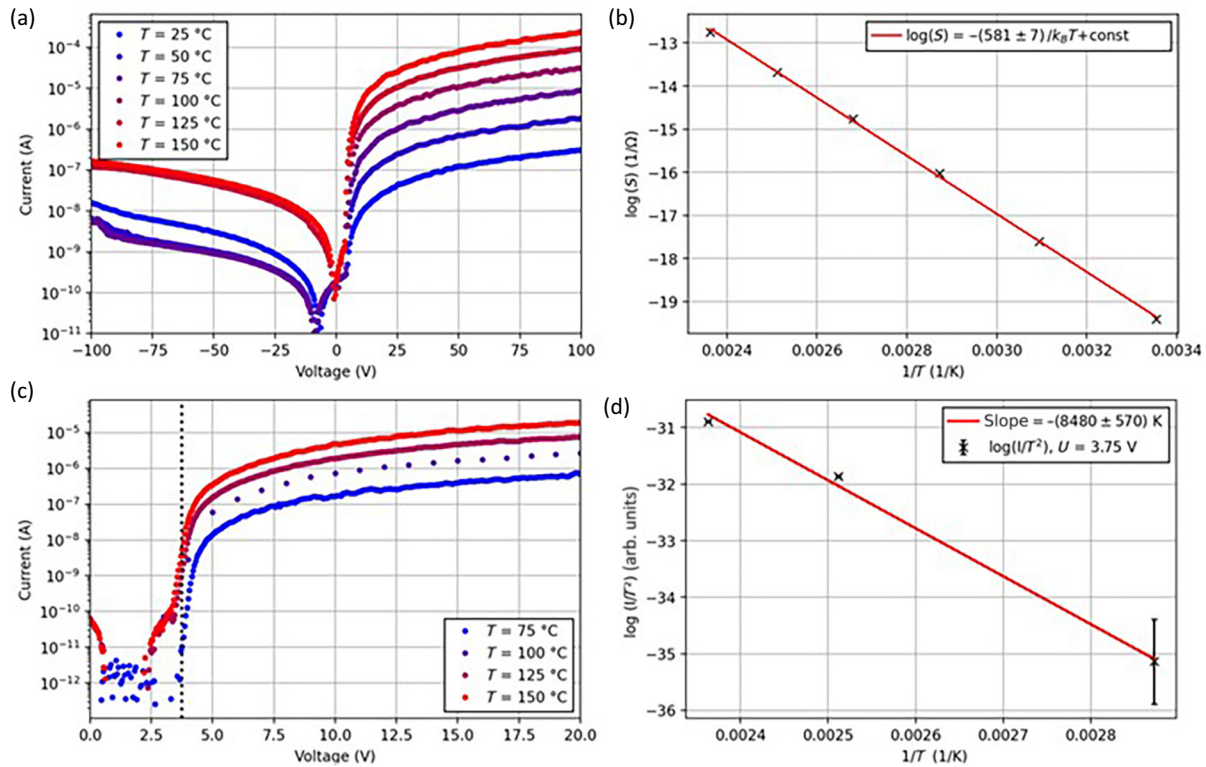


FIG. 3. (a) Raw  $IV$  curves measured at different temperatures. The reverse bias current is dominated by the parallel current through the measurement devices. (b) Natural logarithm of the on-conductance ( $S$ ) as a function of inverse temperature. (c)  $IV$  curves corrected for a parallel resistance of 22.9 GΩ. The black-dotted line is located at 3.75 V; at this voltage, the current is read for the calculation of the barrier height. (d) Temperature dependence of the current over temperature squared as a function of inverse temperature. From the slope, a barrier height for electrons of  $\Phi_{B,e} = 4.48 \pm 0.05 \text{ eV}$  is determined.

measuring device during the experiment. At a temperature of 150 °C, a rectification ratio of  $\sim 1000$  (maximal forward current divided by maximal reverse current) is observed with no sign of an electrical breakdown in the measured voltage range. To characterize the temperature dependence of the forward bias current, the on-state conductance is calculated as the average slope of the  $IV$  curve above 75 V. The conductance ( $S$ ) is plotted in Fig. 3(b) in a linearized form by calculating the natural logarithm as a function of the inverse temperature. A linear function is fitted to this data, resulting in the slope of  $-581 \pm 7$  [meV]/ $k_B T$ , where  $k_B$  is the Boltzmann constant and  $T$  is the temperature, which essentially agrees with the activation energy of phosphorus in *n*-type diamond [15]. The on-state resistance reduces from  $\approx 220$  MΩ at room temperature down to  $\approx 360$  kΩ at 150 °C. As only direct current measurements have been undertaken, the barrier height is estimated from the temperature dependence of the thermionic emission current [39]. Here, the approximation of an ideal diode behavior is made, resulting in a current dependence at  $U = 3.75$  V  $\gg k_B T/q$  of

$$\log\left(\frac{I}{T^2}\right) = \text{const} - \frac{q(\Phi_{B,e} - 3.75 \text{ [V]})}{k_B T}, \quad (2)$$

such that the barrier height can be calculated from the slope obtained by a linear fit to the data obtained from Fig. 3(c) (black-dotted line at 3.75 V). A barrier height for electrons of  $\Phi_{B,e} = 4.48 \pm 0.05$  eV was determined, which corresponds to a barrier height for holes of  $\Phi_{B,h} \approx E_g - \Phi_{B,e} = 0.97 \pm 0.05$  eV. The value of the barrier height for electrons is still close to the previous results of Suzuki *et al.*, where constant values of 4.3 eV have been observed for several metals due to Fermi level pinning by the surface states [40]. This indicates that the removal of surface states needs further improvement.

## B. Electroluminescence studies

The large barrier height for holes does not allow for the observation of bright luminescence from the color centers. The electroluminescence from ensembles of NV color centers is visible even by the bare eye at elevated temperatures and other electroluminescence signals due to the H3 color centers (also named NVN) that are detected even at room temperature (see Supplemental Material [37]). The signal of the SiV color centers is not distinguishable from the phonon sidebands of the stronger NV emission in this sample. In higher silicon-implanted regions, the typical zero-phonon line (ZPL) of the SiV color centers is visible on top of the tail of other emission bands (see Supplemental Material) [37].

Wide-field imaging of the electroluminescence signals as a function of the applied voltage allows for the direct spatial analysis of the emission characteristics across the whole device. Figure 4(a) shows a wide-field image at an

applied voltage of 100 V at 150 °C. The image shows a radially decaying intensity concentrated at the inner Schottky contact, reaching peak values of  $\sim 63$  000 counts with an integration time of 0.5 s. The intensity at the positions of the three white lines ( $x_1$ ,  $x_2$ , and  $x_3$ ) in Fig. 4(a) is averaged over 50 pixels for a smoothing of the data to determine the onset voltage of the electroluminescence at three different locations with increasing distance from the Schottky contact. The determined intensities are plotted in Fig. 4(b) as a function of the applied voltage (colored lines), along with the current through the whole device (black line). All the intensities show an onset at  $\sim 4$  V, indicated by the black-dotted line, which is defined by crossing a stable signal above one count as a threshold. At this point, one can also see that the  $IV$  curve starts to behave with more ohmic characteristics, which indicates a high voltage drop across the Schottky junction and large band bending. At large applied bias voltages, drift currents determine the local charge carrier densities proportional to the voltage. This leads to an almost linear dependence between the applied voltage and the measured electroluminescence signals. As the diode exhibits ohmic behavior in this regime, the current and the signals show a linear dependence as well (see Supplemental Material) [37]. The emission rates are also highly dependent on the location of the color center since the local densities of the minority carriers decrease with distance from the Schottky contact, resulting in different dependencies at the different locations ( $x_1$ ,  $x_2$ , and  $x_3$ ) (see Fig. S3 within the Supplemental Material [37]).

The electroluminescence spectra shown in Figs. 4(c) and 4(d) are recorded at the white  $\times$  marked in Fig. 4(a), which indicates the optical axis of the confocal microscopy setup. The spectra are acquired in an automatic loop by changing the applied forward bias voltage, recording current and spectra at every step with an integration time of 2 s. The spectra at 150 °C and different applied bias voltages [Fig. 4(c)] shows a dominant emission from neutral-charge state NV (i.e., NV<sup>0</sup>) color centers, with a ZPL at  $\sim 580$  nm and a broad phonon-sideband centered at 620 nm. This is due to the fact that a single captured electron cannot provide sufficient energy to transform the color center from the neutral ground state to the negative charge state and, at the same time, bring it to its excited state [21]. Recently, the electroluminescence of NV<sup>-</sup> using a *p-i-n* structure has been reported based on the change in the emission spectrum [20]. Although the signal is mainly dominated by NV<sup>0</sup>, further measurements are required to understand the corresponding photophysics.

Along with the emission from the NV color centers, two other emission bands are observed. The first one is centered at 430 nm and is associated with band-A emission [41]. The second one is centered at  $\sim 510$  nm and relates to the H3 color centers [41]. The observed electroluminescence is the sum of the three color centers' emission spectra,

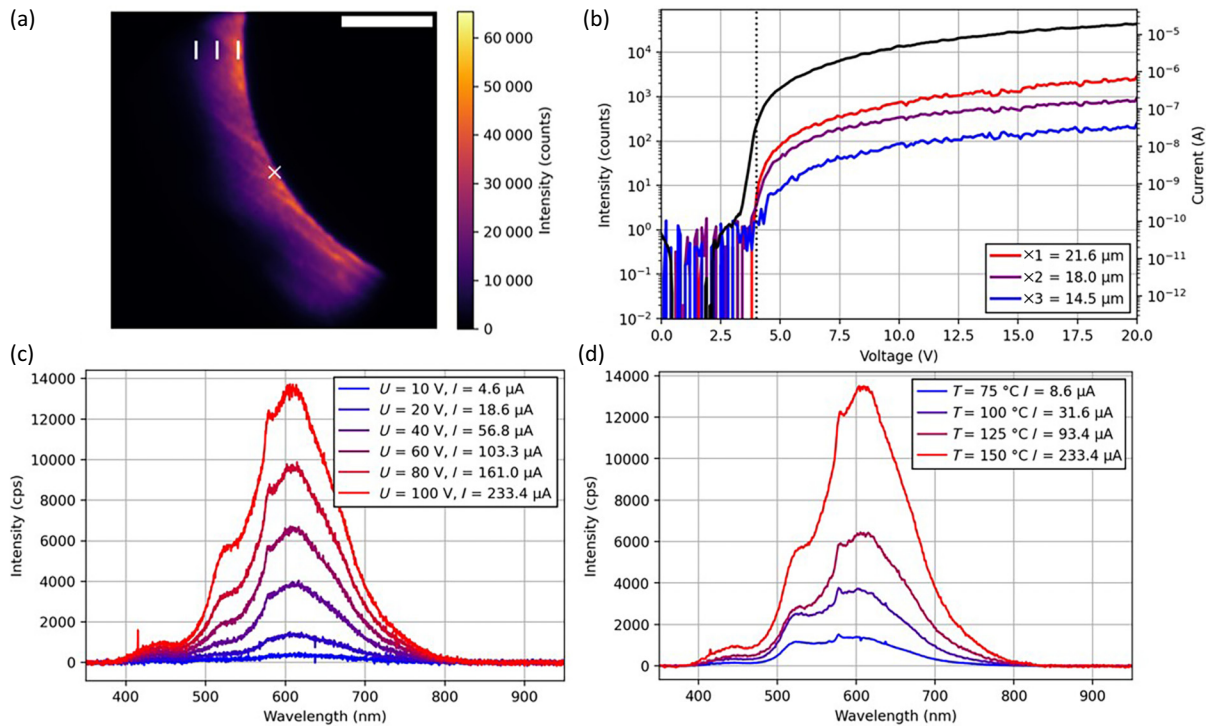


FIG. 4. (a) Wide-field electroluminescence images at 150 °C and applied bias voltages of 100 V. The scalebar in the top right-hand side corner corresponds to a size of 15  $\mu\text{m}$ . The white  $\times$  in the center marks the location of the optical axis, where the electroluminescence spectra are recorded. The three smaller vertical lines indicate the positions where the intensities in (b) are obtained as an average over 50 pixels. (b) Intensities (colored) across the white lines marked in (a) and the current through the whole device (black). Electroluminescence is visible above a turn-on voltage of 4 V (indicated by the black-dotted vertical line). At this point, the  $IV$  curve starts to become ohmic, which indicates a high potential difference across the Schottky barrier. (c) Electroluminescence spectra recorded at different applied bias voltages for a temperature of 150 °C. The center of the collection area is marked by the white  $\times$  in (a). The spectra show a dominant emission from the  $NV^0$  color centers along with the emission from the H3 color centers. (d) Smoothed electroluminescence spectra at an applied bias voltage of 100 V at different temperatures. Due to the increase in temperature, the number of electrons in the  $n$ -type diamond increases and leads to a stronger emission from the  $NV$  color centers compared with the emission from the H3 color centers.

which are visible as different plateaus. While the emission from the  $NV^0$  color centers increases proportional to the current through the device, the emission from the H3 color centers becomes stronger with an increase in the applied voltage. This can be seen by the changes in the spectral shape at different applied bias voltages in Fig. 4(c) and, more clearly, from the different compositions of the spectra at different temperatures in Fig. 4(d). This could be either due to a different excitation scheme of these color centers or a significant amount of the charge carriers moving through the nitrogen-rich HPHT substrate and not only in the  $n$ -type thin film. The latter case could be caused by the lateral geometry of the structure leading to a downstream of holes into the substrate from the edge of the Schottky contact. A reduction of the spacing between the contacts down to 1  $\mu\text{m}$  or less increases the lateral electric field within the  $n$ -type layer, which can confine the charge carriers into the doped film. Figure 4(d) shows that the electroluminescence signal of the  $NV$  color centers increases more strongly with temperature

growth compared with the other emission bands. This agrees with the predictions of Fedyanin and Agio [21] that the increase of charge carriers (mainly electrons) compensates for the reduction in the quantum efficiency. Thus, the excitation of the  $NV$  color centers is limited by the electron capture rather than the hole capture, which should be seen via a saturation behavior of the emission as a function of current. Besides the needed increase in the barrier height for a stronger injection of holes, a further increase in the electron density is required to observe the electroluminescence from the  $NV$  color centers at room temperature.

## VI. CONCLUSIONS

In conclusion, we demonstrated a different approach for the electrical excitation of color centers in a  $n$ -type diamond Schottky configuration and studied its electrical properties and the electroluminescence under different conditions. Barrier heights on the order of 4.5 eV have

been obtained, which allow for only a small injection of holes into the diamond lattice. The observed emission is dominated by nitrogen-related defects ( $H_3$  and  $NV^0$ ). We have shown that the emission from the  $NV$  color centers increases with temperature as the charge carrier density in the  $n$ -type layer increases, which shows that electron capture is still the limiting factor in the emission process. However, our findings provide a perspective for optoelectronics based on color centers in diamond [42]. The N-rich substrate prevented us from observing single-photon emission, but the introduction of a buffer diamond layer or substrate removal would allow one to address single-color centers. Hence, this work is also relevant for efficient electrically driven single-photon sources since the approach can be combined with thin diamond membranes as a host material for the single emitters [43] in combination with planar optical antennas for an efficient light extraction [44,45].

## ACKNOWLEDGMENTS

The authors gratefully acknowledge financial support from the University of Siegen, the German Research Association (DFG) (INST 221/118-1 FUGG, 410405168), the Hasselt University Special Research Fund (BOF), the Research Foundation Flanders (FWO-G0D4920N), and the Methusalem NANO network. The authors also acknowledge INFN-CHNet, the network of laboratories of the INFN for cultural heritage, for their support and precious contributions in terms of instrumentation and personnel.

The authors F.S., A.M.F., and M.A. filed a patent for a diamond LED based on the results of this work (patent pending, DE102021123907.9).

## DATA AVAILABILITY

The data that support the findings of this article are openly available [46].

- [1] B. Darquié, M. P. A. Jones, J. Dingjan, J. Beugnon, S. Bergamini, Y. Sortais, G. Messin, A. Browaeys, and P. Grangier, Controlled single-photon emission from a single trapped two-level atom, *Science* **309**, 454 (2005).
- [2] D. B. Higginbottom, L. Slodička, G. Araneda, L. Lachman, R. Filip, M. Hennrich, and R. Blatt, Pure single photons from a trapped atom source, *New J. Phys.* **18**, 093038 (2016).
- [3] H. G. Barros, A. Stute, T. E. Northup, C. Russo, P. O. Schmidt, and R. Blatt, Deterministic single-photon source from a single ion, *New J. Phys.* **11**, 103004 (2009).
- [4] B. Lounis and W. E. Moerner, Single photons on demand from a single molecule at room temperature, *Nature* **407**, 491 (2000).
- [5] P. Lombardi, M. Trapuzzano, M. Colautti, G. Margheri, I. P. Degiovanni, M. López, S. Kück, and C. Toninelli, A molecule-based single-photon source applied in quantum radiometry, *Adv. Quantum Technol.* **3**, 1900083 (2020).
- [6] I. Aharonovich, S. Castelletto, D. A. Simpson, C.-H. Su, A. D. Greentree, and S. Prawer, Diamond-based single-photon emitters, *Rep. Prog. Phys.* **74**, 076501 (2011).
- [7] S. Castelletto and A. Boretti, Silicon carbide color centers for quantum applications, *J. Phys. Photonics* **2**, 022001 (2020).
- [8] P. Michler, A. Kiraz, C. Becher, W. V. Schoenfeld, P. M. Petroff, L. Zhang, E. Hu, and A. Imamoglu, A quantum dot single-photon turnstile device, *Science* **290**, 2282 (2000).
- [9] Z. Yuan, B. E. Kardynal, R. M. Stevenson, A. J. Shields, C. J. Lobo, K. Cooper, N. S. Beattie, D. A. Ritchie, and M. Pepper, Electrically driven single-photon source, *Science* **295**, 102 (2002).
- [10] T. Heindel, C. Schneider, M. Lermer, S. H. Kwon, T. Braun, S. Reitzenstein, S. Höfling, M. Kamp, and A. Forchel, Electrically driven quantum dot-micropillar single photon source with 34% overall efficiency, *Appl. Phys. Lett.* **96**, 011107 (2010).
- [11] S. Lagomarsino, F. Gorelli, M. Santoro, N. Fabbri, A. Hajeb, S. Sciortino, L. Palla, C. Czelusniak, M. Massi, F. Taccetti, L. Giuntini, *et al.*, Robust luminescence of the silicon-vacancy center in diamond at high temperatures, *AIP Adv.* **5**, 127117 (2015).
- [12] A. Boretti, L. Rosa, A. Mackie, and S. Castelletto, Electrically driven quantum light sources, *Adv. Opt. Mater.* **3**, 1012 (2015).
- [13] M. Petruzzella, F. M. Pagliano, Ž Zobenica, S. Birindelli, M. Cotrufo, F. W. M. Van Otten, R. W. Van Der Heijden, and A. Fiore, Electrically driven quantum light emission in electromechanically tuneable photonic crystal cavities, *Appl. Phys. Lett.* **111**, 251101 (2017).
- [14] Y. Yan and S. Wei, Doping asymmetry in wide-bandgap semiconductors: Origins and solutions, *Phys. Status Solidi B* **245**, 641 (2008).
- [15] S. Koizumi and M. Suzuki, n-Type doping of diamond, *Phys. Status Solidi A* **203**, 3358 (2006).
- [16] A. Lohrmann, S. Pezzagna, I. Dobrinets, P. Spinicelli, V. Jacques, J.-F. Roch, J. Meijer, and A. M. Zaitsev, Diamond based light-emitting diode for visible single-photon emission at room temperature, *Appl. Phys. Lett.* **99**, 251106 (2011).
- [17] N. Mizuuchi, T. Makino, H. Kato, D. Takeuchi, M. Ogura, H. Okushi, M. Nothaft, P. Neumann, A. Gali, F. Jelezko, *et al.*, Electrically driven single-photon source at room temperature in diamond, *Nat. Photonics* **6**, 299 (2012).
- [18] B. Tegetmeyer, C. Schreyvogel, N. Lang, W. Müller-Sebert, D. Brink, and C. E. Nebel, Electroluminescence from silicon vacancy centers in diamond p-i-n diodes, *Diamond Relat. Mater.* **65**, 42 (2016).
- [19] A. M. Berhane, S. Choi, H. Kato, T. Makino, N. Mizuuchi, S. Yamasaki, and I. Aharonovich, Electrical excitation of silicon-vacancy centers in single crystal diamond, *Appl. Phys. Lett.* **106**, 171102 (2015).
- [20] M. Haruyama, H. Kato, M. Ogura, Y. Kato, D. Takeuchi, S. Yamasaki, T. Iwasaki, H. Morishita, M. Fujiwara, N. Mizuuchi, and T. Makino, Electroluminescence of

- negatively charged single NV centers in diamond, *Appl. Phys. Lett.* **122**, 072101 (2023).
- [21] D. Y. Fedyanin and M. Agio, Ultrabright single-photon source on diamond with electrical pumping at room and high temperatures, *New J. Phys.* **18**, 073012 (2016).
- [22] I. A. Khramtsov, M. Agio, and D. Yu. Fedyanin, Dynamics of single-photon emission from electrically pumped color centers, *Phys. Rev. Appl.* **8**, 024031 (2017).
- [23] M. I. Current, Ion implantation of advanced silicon devices: Past, present and future, *Mater. Sci. Semicond. Process.* **62**, 13 (2017).
- [24] R. Rouzbahani, K. J. Sankaran, P. Pobedinskas, and K. Haenen, Advances in *n*-type chemical vapor deposition diamond growth: morphology and dopant control, *Acc. Mater. Res.* **5**, 775 (2024).
- [25] J. Forneris, P. Traina, D. C. Monticone, G. Amato, L. Boarino, G. Brida, I. P. Degiovanni, E. Enrico, E. Moreva, V. Grilj, *et al.*, Electrical stimulation of non-classical photon emission from diamond color centers by means of sub-superficial graphitic electrodes, *Sci. Rep.* **5**, 15901 (2015).
- [26] Y. Guo, W. Zhu, J. Zhao, S. Lin, Y. Yang, L. Lou, and G. Wang, Electroluminescence of NV by impact excitation and Stark shift in a MIM diamond structure, *Appl. Phys. Lett.* **119**, 252102 (2021).
- [27] D. L. Scharfetter, Minority carrier injection and charge storage in epitaxial Schottky barrier diodes, *Solid-State Electron.* **8**, 299 (1965).
- [28] S. Tiwari and D. J. Frank, Empirical fit to band discontinuities and barrier heights in III–V alloy systems, *Appl. Phys. Lett.* **60**, 630 (1992).
- [29] E. H. Rhoderick and R. H. Williams, *Metal-Semiconductor Contacts*, 2nd ed (Clarendon Press; Oxford University Press, Oxford [England]–New York, 1988).
- [30] H. Kageshima and M. Kasu, Origin of Schottky barrier modification by hydrogen on diamond, *Jpn. J. Appl. Phys.* **48**, 111602 (2009).
- [31] K. M. O'Donnell, M. T. Edmonds, A. Tadich, L. Thomsen, A. Stacey, A. Schenk, C. I. Pakes, and L. Ley, Extremely high negative electron affinity of diamond via magnesium adsorption, *Phys. Rev. B* **92**, 035303 (2015).
- [32] W. M. H. Sachtler, G. J. H. Dorgelo, and A. A. Holscher, The work function of gold, *Surf. Sci.* **5**, 221 (1966).
- [33] S. Koizumi, T. Teraji, and H. Kanda, Phosphorus-doped chemical vapor deposition of diamond, *Diamond Relat. Mater.* **9**, 935 (2000).
- [34] A. M. Flatae, S. Lagomarsino, F. Sledz, N. Soltani, S. S. Nicley, K. Haenen, R. Rechenberg, M. F. Becker, S. Sciortino, N. Gelli, *et al.*, Silicon-vacancy color centers in phosphorus-doped diamond, *Diamond Relat. Mater.* **105**, 107797 (2020).
- [35] R. Rouzbahani, S. S. Nicley, D. E. P. Vanpoucke, F. Lloret, P. Pobedinskas, D. Araujo, and K. Haenen, Impact of methane concentration on surface morphology and boron incorporation of heavily boron-doped single crystal diamond layers, *Carbon* **172**, 463 (2021).
- [36] S. Lagomarsino, S. Sciortino, N. Gelli, A. M. Flatae, F. Gorelli, M. Santoro, M. Chiari, C. Czelusniac, M. Massi, F. Taccetti, *et al.*, The center for production of single-photon emitters at the electrostatic-deflector line of the Tandem accelerator of LABEC (Florence), *Nucl. Instrum. Methods Phys. Res., Sect. B* **422**, 31 (2018).
- [37] See Supplemental Material at <http://link.aps.org/supplemental/10.1103/PhysRevApplied.23.054060> for (1) estimation of the NV concentration in the *n*-type layer, (2) hydrogen passivation on the intrinsic diamond, (3) room temperature electroluminescence, (4) current dependence of the emission, and (5) electroluminescence signals in higher implanted regions.
- [38] F. Maier, J. Ristein, and L. Ley, Electron affinity of plasma-hydrogenated and chemically oxidized diamond (100) surfaces, *Phys. Rev. B* **64**, 165411 (2001).
- [39] A. Di Bartolomeo, Graphene Schottky diodes: An experimental review of the rectifying graphene/semiconductor heterojunction, *Phys. Rep.* **606**, 1 (2016).
- [40] M. Suzuki, S. Koizumi, M. Katagiri, T. Ono, N. Sakuma, H. Yoshida, T. Sakai, and S. Uchikoga, Electrical characteristics of *n*-type diamond Schottky diodes and metal/diamond interfaces, *Phys. Status Solidi A* **203**, 3128 (2006).
- [41] H. Kato, M. Wolfer, C. Schreyvogel, M. Kunzer, W. Müller-Sebert, H. Obloh, S. Yamasaki, and C. Nebel, Tunable light emission from nitrogen-vacancy centers in single crystal diamond PIN diodes, *Appl. Phys. Lett.* **102**, 151101 (2013).
- [42] D. Yu. Fedyanin, Optoelectronics of color centers in diamond and silicon carbide: from single-photon luminescence to electrically controlled spin qubits, *Adv. Quantum Technol.* **4**, 2100048 (2021).
- [43] A. M. Flatae, F. Sledz, H. Kambalathmana, S. Lagomarsino, H. Wang, N. Gelli, S. Sciortino, E. Wörner, C. Wild, B. Butz, and M. Agio, Single-photon emission from silicon-vacancy color centers in polycrystalline diamond membranes, *Appl. Phys. Lett.* **124**, 094001 (2024).
- [44] H. Galal and M. Agio, Highly efficient light extraction and directional emission from large refractive-index materials with a planar Yagi-Uda antenna, *Opt. Mater. Express* **7**, 1634 (2017).
- [45] H. Galal, A. M. Flatae, S. Lagomarsino, G. Schulte, C. Wild, E. Wörner, N. Gelli, S. Sciortino, H. Schönherr, L. Giuntini, and M. Agio, Highly efficient light extraction and directional emission from diamond color centers using planar Yagi-Uda antennas, [arXiv:1905.03363](https://arxiv.org/abs/1905.03363).
- [46] F. Sledz, Raw data and simulation results for the electrical excitation of color centers in a *n*-type diamond Schottky diode, <https://doi.org/10.25819/VYWD4QUJ3XQ9VWPW>.